Title

Granulosa cell and oocyte mitochondrial abnormalities in a mouse model of fragile X primary ovarian insufficiency

Journal

Molecular Human Reproduction, 22(6)

ISSN

1360-9947

Authors

Dioguardi, Carola Conca
Uslu, Bahar
Haynes, Monique
et al.

Publication Date

2016-06-01

DOI

10.1093/molehr/gaw023

Peer reviewed

Molecular Human Reproduction, Vol.22, No.6 pp. 384–396, 2016
Advanced Access publication on March 9, 2016 doi:10.1093/molehr/gaw023

molecular human reproduction

ORIGINAL RESEARCH

Granulosa cell and oocyte mitochondrial abnormalities in a mouse model of fragile X primary ovarian insufficiency

Carola Conca Dioguardi[1,2,3], Bahar Uslu[1,2], Monique Haynes[1,2], Meltem Kurus[4], Mehmet Gul[5], De-Qiang Miao[1,2], Lucia De Santis[6], Maurizio Ferrari[7], Stefania Bellone[1,8], Alessandro Santin[1,8], Cecilia Giulivi[9], Gloria Hoffman[10], Karen Usdin[11], and Joshua Johnson[1,2,*]

[1]Department of Obstetrics, Gynecology, & Reproductive Sciences, Yale School of Medicine, New Haven, CT, USA [2]Division of Reproductive Endocrinology and Infertility, Yale School of Medicine, New Haven, CT, USA [3]Vita-Salute San Raffaele University/IRCCS San Raffaele Hospital, Milan, Italy [4]Department of Histology & Embryology, Izmir Katip Celebi University School of Medicine, Izmir, Turkey [5]Department of Histology & Embryology, Inonu University School of Medicine, Malatya, Turkey [6]Department of Obstetrics & Gynecology, IVF Unit, Vita-Salute San Raffaele University/IRCCS San Raffaele Hospital, Milan, Italy [7]Laboratory of Clinical Molecular Biology and Cytogenetics, Vita-Salute San Raffaele University/IRCCS San Raffaele Hospital, Milan, Italy [8]Division of Gynecologic Oncology, Yale School of Medicine, New Haven, CT, USA [9]Department of Molecular Biosciences, M.I.N.D. Institute, University of California-Davis, Davis, CA, USA [10]Department of Biology, Morgan State University, Baltimore, MD, USA [11]Laboratory of Cellular and Molecular Biology, NIH/NIDDK, Bethesda, MD, USA

*Correspondence address. E-mail: josh.johnson@yale.edu

Submitted on December 1, 2015; resubmitted on February 4, 2016; accepted on March 4, 2016

STUDY HYPOTHESIS: We hypothesized that the mitochondria of granulosa cells (GC) and/or oocytes might be abnormal in a mouse model of fragile X premutation (FXPM).

STUDY FINDING: Mice heterozygous and homozygous for the FXPM have increased death (atresia) of large ovarian follicles, fewer *corpora lutea* with a gene dosage effect manifesting in decreased litter size(s). Furthermore, granulosa cells (GC) and oocytes of FXPM mice have decreased mitochondrial content, structurally abnormal mitochondria, and reduced expression of critical mitochondrial genes. Because this mouse allele produces the mutant *Fragile X mental retardation 1 (Fmr1)* transcript and reduced levels of wild-type (WT) Fmr1 protein (FMRP), but does not produce a Repeat Associated Non-ATG Translation (RAN)-translation product, our data lend support to the idea that *Fmr1* mRNA with large numbers of CGG-repeats is intrinsically deleterious in the ovary.

WHAT IS KNOWN ALREADY: Mitochondrial dysfunction has been detected in somatic cells of human and mouse FX PM carriers and mitochondria are essential for oogenesis and ovarian follicle development, FX-associated primary ovarian insufficiency (FXPOI) is seen in women with FXPM alleles. These alleles have 55–200 CGG repeats in the 5′ UTR of an X-linked gene known as *FMR1*. The molecular basis of the pathology seen in this disorder is unclear but is thought to involve either some deleterious consequence of overexpression of RNA with long CGG-repeat tracts or of the generation of a repeat-associated non-AUG translation (RAN translation) product that is toxic.

STUDY DESIGN, SAMPLES/MATERIALS, METHODS: Analysis of ovarian function in a knock-in FXPM mouse model carrying 130 CGG repeats was performed as follows on WT, PM/+, and PM/PM genotypes. Histomorphometric assessment of follicle and *corpora lutea* numbers in ovaries from 8-month-old mice was executed, along with litter size analysis. Mitochondrial DNA copy number was quantified in oocytes and GC using quantitative PCR, and cumulus granulosa mitochondrial content was measured by flow cytometric analysis after staining of cells with Mitotracker dye. Transmission electron micrographs were prepared of GC within small growing follicles and mitochondrial architecture was compared. Quantitative RT–PCR analysis of key genes involved in mitochondrial structure and recycling was performed.

MAIN RESULTS AND THE ROLE OF CHANCE: A defect was found in follicle survival at the large antral stage in PM/+ and PM/PM mice. Litter size was significantly decreased in PM/PM mice, and *corpora lutea* were significantly reduced in mice of both mutant genotypes. Mitochondrial DNA copy number was significantly decreased in GC and metaphase II eggs in mutants. Flow cytometric analysis revealed that PM/+ and PM/PM animals lack the cumulus GC that harbor the greatest mitochondrial content as found in wild-type animals. Electron microscopic evaluation of GC of small growing follicles revealed mitochondrial structural abnormalities, including disorganized and vacuolar cristae. Finally, aberrant mitochondrial gene expression was detected. Mitofusin 2 *(Mfn2)* and Optic atrophy 1 *(Opa1)*, genes involved in mitochondrial fusion and

structure, respectively, were significantly decreased in whole ovaries of both mutant genotypes. Mitochondrial fission factor 1 *(Mff1)* was significantly decreased in PM/+ and PM/PM GC and eggs compared with wild-type controls.

LIMITATIONS, REASONS FOR CAUTION: Data from the mouse model used for these studies should be viewed with some caution when considering parallels to the human FXPOI condition.

WIDER IMPLICATIONS OF THE FINDINGS: Our data lend support to the idea that *Fmr1* mRNA with large numbers of CGG-repeats is intrinsically deleterious in the ovary. FXPM disease states, including FXPOI, may share mitochondrial dysfunction as a common underlying mechanism.

LARGE SCALE DATA: Not applicable.

STUDY FUNDING AND COMPETING INTEREST(S): Studies were supported by NIH R21 071873 (J.J./G.H), The Albert McKern Fund for Perinatal Research (J.J.), NIH Intramural Funds (K.U.), and a TUBITAK Research Fellowship Award (B.U.). No conflict(s) of interest or competing interest(s) are noted.

Key words: fragile X primary ovarian insufficiency / fragile X premutation / ovary / oocyte / follicle / fertility / atresia / mitochondria

Introduction

Fragile X primary ovarian insufficiency (FXPOI) is the most common known inheritable form of ovarian dysfunction. FXPOI is a member of the fragile X-related disorders (FXDs). This group of genetic disorders arises from an increase or 'expansion' in the size of a CGG microsatellite in the 5′ UTR region of the X-linked *FMR1* gene at Xq27.3. CGG expansions between 55 and 200 repeats are known as premutation (PM)-length alleles. PM alleles are prone to further intergenerational expansion through the maternal germ-line, resulting in alleles that can have >200 repeats. Such alleles are referred to as full mutation (FM) alleles and are associated with fragile X syndrome (FXS), the most common heritable form of intellectual disability and the most common monogenic cause of autism. FXPOI, and an adult onset form of neurodegeneration known as fragile X-associated tremor/ataxia syndrome (FXTAS) are associated with PM-length repeats.

The symptoms of FXPOI include fertility problems, menstrual cycle irregularities and menopause before the age of 40. The incidence of FXPOI in the female PM population is approximately 28% (Welt *et al.*, 2004) and FXPOI is thought to constitute 11.5% of familial cases of infertility and 3.5% of idiopathic cases (Murray *et al.*, 1998; Allen *et al.*, 2007). How this reproductive pathology arises in PM carriers is essentially unknown. Information is available, however, about the cellular consequences of aberrant PM transcription and translation near the *FMR1* gene.

Unlike FM alleles that undergo repeat-mediated gene silencing (Pieretti *et al.*, 1991; Sutcliffe *et al.*, 1992), PM alleles are active and actually show elevated *FMR1* mRNA levels (Tassone *et al.*, 2000, 2007). By analogy with myotonic dystrophy type 1 and 2 that result from expression of a CUG-containing and a CCUG-containing transcript respectively (Handa *et al.*, 2005; McLeod *et al.*, 2005; Wojciechowska and Krzyzosiak, 2011; Hagerman and Hagerman, 2013), it has been suggested that the PM transcript may bind and sequester factors important for cell function (Sellier *et al.*, 2010). Indeed abnormalities consistent with the sequestration of factors like Src-Associated substrate in Mitosis of 68 kDa (SAM68), and Drosha/Ribonuclease III (DROSHA) have been observed in PM cells (Sellier *et al.*, 2010, 2013).

In addition to potential pathology related to protein sequestration, a form of repeat-associated non-AUG (RAN) translation has also been shown to occur in human PM cells (Todd *et al.*, 2013). This translation generates a protein, Fragile x mental retardation—PolyG (FMRPolyG), that containing a lengthy polyglycine tract that is toxic to a number of cell types (Todd *et al.*, 2013; Oh *et al.*, 2015). However, the relative contribution of RNA sequestration (of essential factors) and RAN translation (of the toxic FMRPolyG) to PM pathology is unknown. Previous work on two mouse PM models generated on different genetic backgrounds (see (Pastore and Johnson, 2014) for a review) showed evidence of ovarian dysfunction. One of these mouse strains, FXPM 130R, has ~130 repeats and makes a PM transcript but not a PM RAN product (Todd *et al.*, 2013). That mouse showed evidence of ovarian abnormalities (Hoffman *et al.*, 2012), raising the possibility that the PM transcript itself has pathological consequences in the ovary.

A vital interplay between oocytes and their associated granulosa cells (GC) occurs during follicle growth from the arrested primordial follicle stage to the ovulatory stage (Albertini and Barrett, 2003; Wigglesworth *et al.*, 2015). During folliculogenesis, oocyte mitochondria become more abundant and experience dynamic changes as they mature (Van Blerkom, 2004, 2011). Reactive oxygen species (ROS) have positive developmental roles in the ovary, functioning as a necessary signal for ovulation (de Lamirande and Gagnon, 1994; Behrman *et al.*, 2001) and regulating corpus luteum function and regression (Carlson *et al.*, 1993). However, if the balance between oxidative stress and antioxidant defenses is altered, for example by chemical toxicants, ovarian compromise can result. There is strong evidence that ROS are involved in the initiation of apoptosis in antral follicles upon exposure to chemicals (Luderer, 2014). Furthermore, a significant decrease in fertilization rate and in the quality of embryos in IVF cycles is seen when increased oxidative DNA damage was generated (Seino *et al.*, 2002). More recent findings suggest that excessive ROS generation in GC correlate with significant morphological abnormalities, decreased mitochondrial membrane potential, and higher levels of DNA fragmentation which correlated with poorer quality eggs and embryos (Karuputhula *et al.*, 2013).

Differences between oxidative stress markers and mitochondrial parameters are seen between women with compromised ovarian function and normal controls. Serum levels of multiple oxidative stress genes are elevated in women with primary ovarian insufficiency (POI) compared with BMI- and age-matched controls (Tokmak *et al.*, 2015). In addition, the cumulus GC of patients with diminished ovarian reserve had reduced mitochondrial DNA (mtDNA) content, and lower levels of peroxisome proliferator-activated receptor γ coactivator

1 alpha (PPARGC-1A) than patients with normal ovarian reserve (Boucret et al., 2015). Genetic factors that might predispose a woman to exhibit such changes that accompany compromised ovarian function have not, however, been reported.

Prior studies have suggested the PM allele causes mitochondrial dysfunction in the brains and fibroblasts of human PM carriers and in the livers of a PM mouse model (Ross-Inta et al., 2010; Kaplan et al., 2012a; Hukema et al., 2014). We thus tested whether mitochondrial content and/or structure were different in the ovaries of FXPM 130R mice. While women with FXPOI have only one PM allele, we examined both mice heterozygous and homozygous for the PM. We rationalized that homozygous mice might have an exaggerated ovarian phenotype compared to that seen in heterozygote animals.

Materials and Methods

Ethical approval

Mice were handled and tissues were collected in accordance with an active protocol under the auspices of the Yale IACUC.

Mice and tissue collection

Where applicable, oviduct/ovary complexes were collected via ventral laparotomy and put into dishes containing handling solution (DMEM, 10% FBS). For ovary specimens, unstimulated mice were used. Oviducts and connecting fat were removed under the microscope, and the ovaries were released from the ovarian bursa. Metaphase II (MII) eggs and cumulus GC were collected after 'superovulation' with Pregnant Mare's Serum Gonadotrophin (PMSG) and human Chorionic Gonadotrophin (hCG) (Sigma Aldrich, USA). In order to decrease blood contamination in GC preparations, every oviduct was isolated from each ovary and washed in 1× PBS. The washed oviduct was then immersed in a solution containing handling medium and 0.3 mg/ml of hyaluronidase (MP Biomedicals, LLC, USA). The oviduct was then cut and the cumulus-oocyte-complexes (COC) were squeezed out. COC were incubated for 8 min at 37°C in order to separate GC and eggs; MII eggs were washed in handling medium and collected and processed for DNA/RNA extraction. The remaining media and GC were collected in a 1.5 ml vial and centrifuged at 500 RCF for 5 min. The supernatant was removed and the pellet containing cumulus GC was re-suspended in 1 ml of handling medium. To avoid clusters of GC, the obtained suspension was gently mixed using a pipette and filtered with a 70 μm filter. After filtration, cells were counted using a Burker chamber and at least 20 000 cells were immediately used to perform each assay. Cell aliquots used for qPCR were stored in RNAlater@ (Life Technologies, USA) at −80°C until use.

Histopathological examination

Fresh ovaries from WT, *PM/+*, and *PM/PM* mice ($n = 4$ per group) were extracted and cleaned from the fat, rinsed in PBS and fixed in Dietrich's fixative (30% Ethanol [EtOH] v/v, 10% Formalin, v/v—using aqueous 37% Formaldehyde solution, 2% Glacial Acetic Acid, v/v, filtered prior to use) overnight. Ovaries were then be transferred into 70% EtOH and embedded in paraffin. 5 μm serial sections were cut and placed onto glass slides (Superfrost/Plus Microscope slides-precleaned; #12-550-15; Fisher Scientific, USA). Slides were warmed, dewaxed with Xylenes (3 times × 5 min.) and rehydrated through an increasing alcohol series up to distilled water. The slides were rinsed in PBS, then stained in Weigert's Iron Hematoxylin (1:1 mixture of Solution A and Solution B. Solution A: Weigert's Iron Solution B: Ferric chloride, 29% aqueous 4 ml, Hematoxylin 1 g in 95% ethanol) for 10 min. Picric Acid (saturated aqueous) Methyl Blue (0.4 mg/ml) counterstaining followed for 6 min. To dehydrate, clean and coverslip the slides, they were put in 95%, then 100% EtOH, then in Xylenes; finally, 1–2 drops of mounting medium (Cytoseal-60 Low Viscosity # 8310-16; Richard-Allan Scientific, USA) were applied and specimens were coverslipped.

Histomorphometric analyses and litter size determination

After specimen coding and blinding, follicles at each developmental stage were counted in every fifth serial section, with raw numbers multiplied by 5 as previously described (Tilly, 2003; Johnson et al., 2004). Criteria for follicle categorization are summarized as follows: a follicle was considered primordial if a single layer of flattened pre-GC surrounded the oocyte. Primary follicles had a single layer of cuboidal GC. The transition to secondary follicle was recognized by the appearance of a second layer of cuboidal GC with no antrum present. Pre-antral follicles had three or more layers of cuboidal GC layers with no antrum present. Antral follicles have multiple cuboidal GC layers with the presence of a visible antral cavity. To avoid double counting, only follicles that contained an oocyte with its nucleus visible in the counted plane were counted. Data for follicle, *zona pellucida* remnant, *corpora lutea* counting and litter size analysis are presented as boxplots where the sample minimum is the horizontal line at the bottom of each plot; the lower limit of the box in each figure is the lower quartile; the heavy line inside each box is the sample median; the upper limit of each box is the upper quartile, and; the horizontal line at the top of each plot is the sample maximum.

Transmission electron microscopy

For electron transmission microscopic examination, samples of ovaries from wild-type, *PM/+* and *PM/PM* mice ($n = 3$ per genotype) were fixed in 2.5% glutaraldehyde (Merck, Germany) buffered with 0.2 M $NaH_2PO_4 + NaHPO_4$ (pH 7.4) and post-fixed in 1% Osmium tetroxide (OsO4) (Merck, Germany). After dehydration in acetone, tissues were embedded in Araldite CY 212. Ultrathin sections were stained with uranyl acetate and lead citrate and examined using a Zeiss Libra 120 transmission electron microscope (Carl Zeiss NTS GmBH, Oberkochen, Germany).

RNA and DNA extraction from mouse tissues

RNA and DNA were extracted using an AllPrep DNA/RNA/Protein Mini kit (Qiagen, USA), according to slightly modified instructions. Whole ovaries, GC, or oocytes (collected fresh or previously stored at −80°C) were disrupted using a BeadBeater sample homogenizer (Biospec Products, USA) for 3 min at maximum speed. The resulting homogenate was briefly centrifuged, then added to an AllPrep DNA spin column according to instructions. RNA was extracted first while DNA was kept at RT until the extraction. In order to increase the RNA concentration, 30–60 microliters of water were added, depending on the type of sample. Finally, RNA and DNA samples were quantified using Nanodrop system (Nanodrop2000c, ThermoScientific), USA; RNA was stored at −80°C and DNA at −20°C until use.

Real-time PCR

To prepare cDNA, 0.5 μg of ovary RNA and 0.1 μg of MII and cumulus GC RNA were reverse transcribed (RT) using Superscript II Reverse Transcriptase (Invitrogen, USA) and random primers (Promega, USA). Negative control mock RT samples were also prepared from each RNA sample where the RT enzyme was omitted from the reaction. RT and mock reaction mixtures were incubated at 65°C for 5 min, 25°C for 10 min, followed by 50 min at 42°C; finally, the enzyme was inactivated by incubation at 95°C for 15 min.

qRT–PCR was performed using a StepOne Plus Thermal Cycler Software v2.3 (Applied Biosystems, USA) and all samples were assayed in triplicate. Two microliters of the single stranded cDNA obtained were mixed with 10 μl of iQ SYBR Green Supermix (Bio-Rad, USA), 1 μM of each forward and reverse primer. Primers used were purchased from Integrated DNA Technologies (IDT; Coralville, IA); sequences are listed in Table I. Thermal cycling conditions were as follows: 5 min at 95°C followed by 40 cycles (95°C 15 s, 60°C 1 min). β-actin was used as a reference gene. The calculation of threshold cycle (Ct) values was performed using the StepOne Plus Software v2.3 (Applied Biosystems) after automatic baseline and threshold selection. Relative expression levels were calculated using the $2-\Delta\Delta CT$ method, and data are presented as the mean ± the standard error of the mean. In each experiment, mock RT samples corresponding to each cDNA sample were also analyzed and were found to generate negligible non-specific PCR product(s).

Evaluation of mitochondrial DNA copy number

qPCR-based mitochondrial DNA (mtDNA) quantification was performed with two different primer sets for genomic and mitochondrial loci in GC and MII eggs, as previously described (Sahin *et al.*, 2011). The reaction was performed using a StepOne Plus Software v2.3 (Applied Biosystems) and assayed in triplicate. Two microliters of DNA were mixed with 10 μl of iQ SYBR Green Supermix (Bio-Rad), 0.5 μl of primer forward and reverse at 1 μM. The thermal cycling conditions were 5 min at 95°C followed by 40 cycles (95°C 15 s, 60°C, 1 min). mtDNA copy number is presented as barplots of the mean ± the standard error of the mean.

Flow cytometry analysis of mitochondrial content

GC (≥10 000) from wild type, heterozygous and homozygous mice were dyed with either Mitotracker@ Green FM (Life Technologies, #M-7514, USA) for 20 min at 37°C in the dark. Live cells were assessed for Mitotracker@ Green signal after re-suspension in 200 μl of 1× PBS, followed by and analysis on a FACSCalibur Flow Cytometer (Becton Dickinson, USA), using CellQuest software. Mitochondrial mass data are presented as a boxplot where the whiskers represent sample minimum and maximum; the lower limit of the box in each figure is the lower quartile; the heavy line inside each box is the sample median; the upper limit of each box is the upper quartile.

Statistical analyses

R (R Project, 2015) and GraphPad Prism (GraphPad Software, Inc., USA) software were used for statistical analyses and plot production. ANOVA multiple group analyses followed by Bonferroni *post hoc* testing were used to compare outcomes, with $P < 0.05$ used as the cutoff for significance and to accept or reject null hypotheses where means were compared.

Results

Figure 1 summarizes the results of follicle counts from FXPM animals at 8 months of age performed in our laboratory. Hypothesizing that homozygosity for the PM would exacerbate any ovarian phenotype, we included *PM/PM* animals in our analysis, an approach that had not been performed in prior studies (Hoffman *et al.*, 2012). In accordance with the prior studies, no difference in the mean number of primordial (A) or immature growing follicles (primary, secondary, and small pre-antral stages; B–D) was found between WT and *PM/+* animals. While no significant difference was seen between *PM/PM* animals and the two other genotypes, much greater variability was seen in follicle number between the individual homozygous PM mouse replicates than the other genotypes. We estimated the amount of replicate variability by calculating the Coefficient of Variation (CV) for WT and PM ovaries, and calculated the ratio of PM to WT CV (Table II). For most *PM/+* and all *PM/PM* histomorphometric measures, the CV ratio was greater than one.

Table I PCR primers used for studies.

Experiment	Gene name	Forward/reverse	Primer sequence (5′ → 3′)
mtDNA PCR	*Cox I*	F	CTGAGCGGGAATAGTGGGTA
		R	TGGGGCTCCGATTATTAGTG
	β-globin	F	GCACCTGACTGATGCTGAGAA
		R	TTCATCGGCGTTCACCTTTCC
qRT–PCR	*β-actin*	F	GCCCTGAGGCTCTTTTCCAG
		R	TGCCACAGGATTCCATACCC
	Drp I	F	TCCCAATTCCATTATCCTCGC
		R	CATCAGTACCCGCATCCATG
	Fis I	F	AGCTGGTTCTGTGTCCAAG
		R	TGTTCCTCTTTGCTCCCTTTG
	Mff	F	CTAATCTTTCCTCTGCCCGTG
		R	GATGAGGATTAGAAGTGGCGG
	Mfn1	F	GGATAATGCAGCCCAGGAG
		R	GACAGAGATTAGTTTCCAGCCC
	Mfn2	F	CATCCCCAGTTGTCCTCAAG
		R	TTCAAGCCGTCTATCATGTCC
	Opa 1	F	GTGTGCTGGAAATGATTGCTC
		R	TGGTGAGATCAAATTCCCGAG
	Prdx5	F	GGAGTCCCTGGGGCATTTAC
		R	AACGCTCAGACAGGCCACCA

Cox I, cytochrome c oxidase I; Drp I, Dynamin 1-like 1; Fis I, Fission 1; Mff, mitochondrial fission factor; Mfn I, Mitofusin-1; Mfn2, Mitofusin-2; Opa I, optical atrophy 1; Prdx5, peroxiredoxin 5.

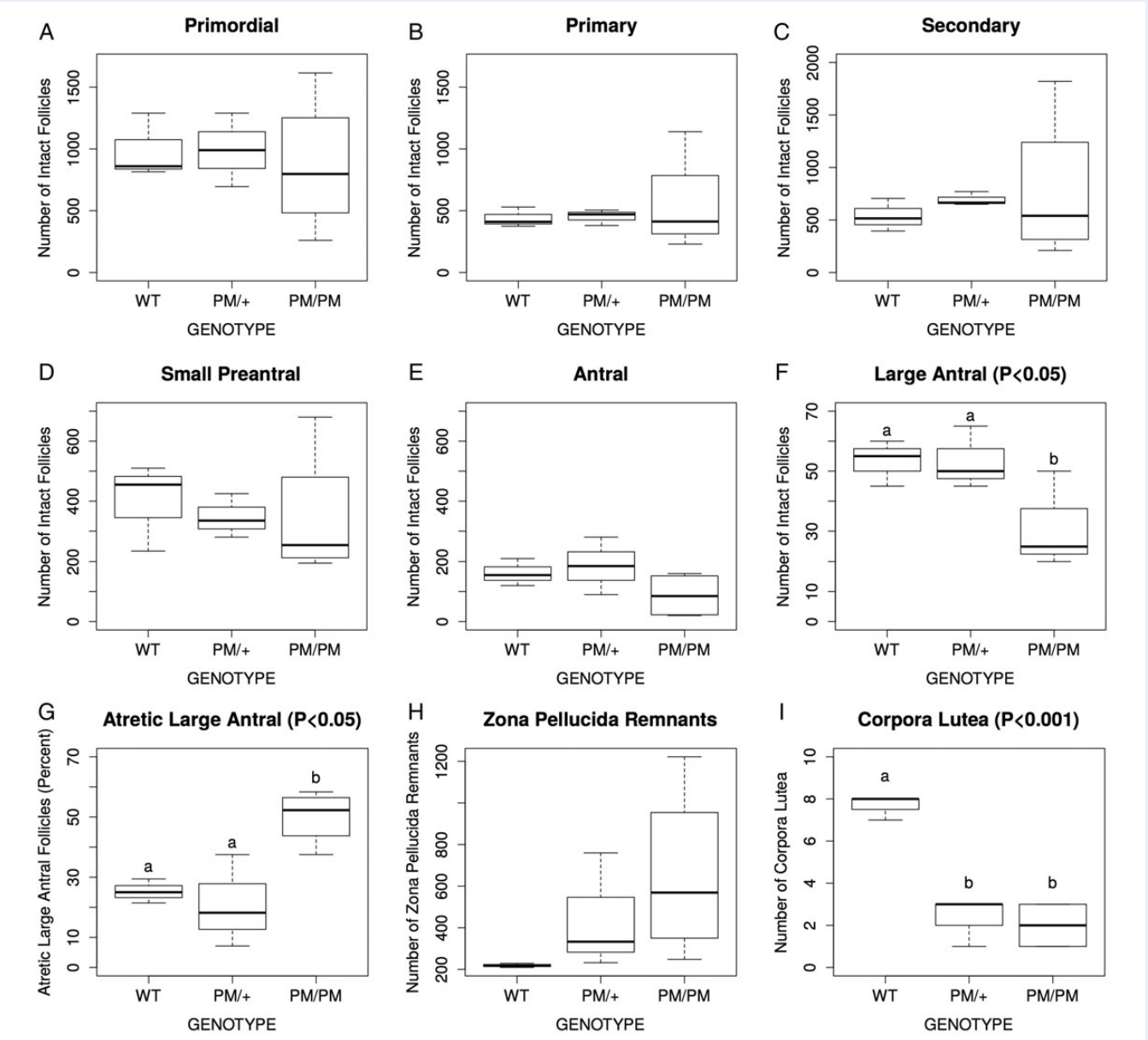

Figure 1 Histomorphometric analysis of follicle number, atresia, and *corpus luteum* number of 8-month-old FXPM mutants and WT control animals. Quantification of intact primordial, primary, secondary, pre-antral, antral, and large antral/periovulatory follicles per ovary ($n = 4$ per geno-type) is shown in (**A**)–(**F**). Follicle atresia was evaluated by counting atretic large antral follicles (**G**) and *zona pellucida* remnants (ZPR, **H**). *Corpus luteum* (CL) number is shown in (**I**). Note increased variability in the number of PM follicles, ZPR, and CL (see also Table II). Statistically different means, where applicable, are denoted by letters 'a' and 'b', with P-values shown above each plot as calculated by ANOVA analysis.

Significant differences in mean follicle number only became apparent as follicles grew to reach the large antral stage of development (E), with *PM/PM* animals demonstrating a decline that was not significant. At the large antral stage, significantly fewer follicles were present in *PM/PM* animals compared with the other genotypes (F). Consistent with this observation, the number of large antral follicles scored as atretic (e.g. dying) was significantly increased in *PM/PM* animals (G), but not in *PM/+* animals. This was consistent with the prior publication where homozygous 130R animals were also found to have elevated numbers of atretic large follicles compared with wild-type controls (Hoffman *et al.*, 2012). Another measurement that can be used to estimate the number of mature follicles that died *via* atresia is counting the number of *zona pellucida* remnants (ZPR; Panel H) (Myers *et al.*, 2004). Each of the PM genotypes exhibited increased numbers of ZPR, compared with WT controls. Here again, while the median numbers of ZPR were not significantly different between the genotypes, the variation in ZPR between ovaries of the individual PM animals was much greater than that of the WT controls (Table II).

Corpora lutea (CL) are ovarian structures that develop from remaining follicle cells after ovulation, supporting pregnancy should conception

Table II Coefficient of variation comparison for histomorphometric analyses in Fig. 1.

Category/genotype	Coefficient of variation ratio mutant: wild-type	
	PM/+	*PM/PM*
Primordial	1.1	2.5
Primary	0.8	4.0
Secondary	0.3	3.2
Small pre-antral	0.6	1.8
Antral	1.8	3.1
Large antral	1.4	3.2
Zona pellucida remnants	13.9	14.1
Corpora lutea	6.6	7.7
Mean CV Ratio	**3.2**	**4.5**

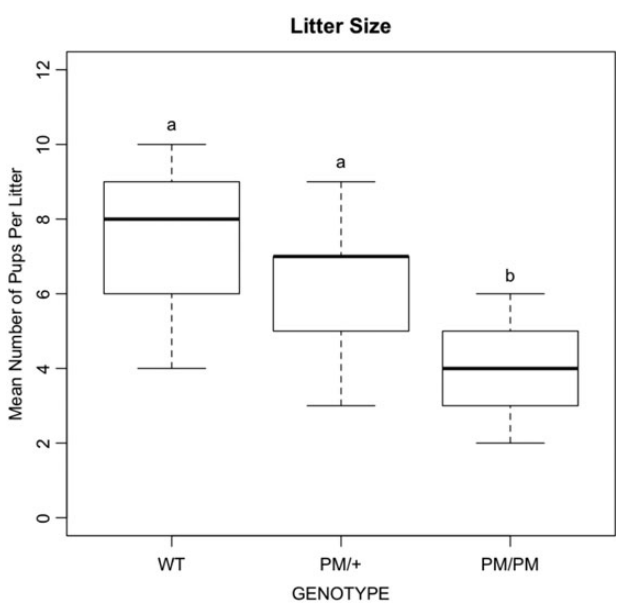

Figure 2 Determination of litter size in FXPM carrier mice versus WT controls. The number of pups produced per litter when mutant ($n = 15$ PM/+ and 10 PM/PM) and WT ($n = 14$) females were crossed to WT males of proven fertility is shown. Statistically different means, are denoted by letters 'a' and 'b' ($P < 0.05$, calculated using ANOVA analysis).

occur. Significantly fewer CL (Fig. 1I) were found in *PM/+* and *PM/PM* ovaries compared with WT controls. And as seen for the different follicle classes, higher variation between animals was noted for CL number in PM animals versus WT (Table II).

Consistent with smaller numbers of CL per ovary, the fecundity of both *PM/+* and *PM/PM* mice were diminished compared with WT mice (Fig. 2). In a breeding trial using 9 rotating males of proven fertility, WT females delivered a mean 7.4 ± 0.4 pups per litter (5 mothers, $n = 14$ litters), *PM/+* 6.1 ± 0.5 pups per litter (5 mothers, $n = 15$ litters), and *PM/PM* 4.3 ± 0.4 pups per litter (5 mothers, $n = 15$ litters). Unlike a prior report where *PM/+* mice with 90 CGG repeats (on a different genetic background) were found to have significantly fewer pups per litter (Lu *et al.*, 2012), only the *PM/PM* mice in our trial reached significance.

Table III Granulosa cell type used for each experiment.

Experiment (figure)	Follicle stage
Mitochondrial DNA copy number (Fig. 3B)	Cumulus/ovulated
Mitochondrial mass assessment by flow cytometry (Fig. 3C)	Cumulus/ovulated
Transmission electron microscopic analysis of mitochondria (Fig. 4)	Pre-antral follicle GC
qRT–PCR gene expression analyses (Fig. 6)	Cumulus/ovulated

Because mitochondrial dysfunction has been detected in somatic cells of human and mouse PM carriers (Ross-Inta *et al.*, 2010; Kaplan *et al.*, 2012a; Hukema *et al.*, 2014) and mitochondria are essential for oogenesis and ovarian follicle development (Van Blerkom, 2004, 2011; Boucret *et al.*, 2015), we hypothesized that the mitochondria of GC and/or oocytes might be abnormal in our mouse PM model. Initial experiments used ovulated cumulus granulosa cells (GC; see Table III for GC types used in each experiment) and MII eggs. We reasoned that if abnormalities were detected in ovulated PM cumulus GC, the same cell type could be assessed in future studies of human carriers undergoing clinical *in vitro* fertilization cycles. We started with the determination of mtDNA copy number. Quantitative PCR (qPCR) using primers specific for the mitochondrial gene *Cox I* and the nuclear housekeeping gene *β-globin* as a normalizing control was performed (Sahin *et al.*, 2011). Both PM genotypes exhibited decreased mtDNA copy number relative to WT controls (Fig. 3A and B). PM GC expressed about three-quarters of the mtDNA detected in WT cells, while mutant MII eggs expressed less than half of the mtDNA of WT eggs. As a further quantitative evaluation of mitochondrial content in cumulus GC, we used a flow cytometric approach using a mitochondria-specific fluorescent probe, Mitotracker@ Green. This probe detects both polarized and unpolarized mitochondria.

After loading cumulus GC isolated from WT and animals of each PM genotype with Mitotracker@ Green, we performed flow cytometric measurement of fluorescence. This mitochondria-specific dye is routinely used in this fashion for the determination of relative mitochondrial mass in individual cells (Addabbo *et al.*, 2009). Measuring a minimum of 10 000 viable cells per sample in three separate experiments, we determined mean fluorescence for cells of each genotype. We found that *PM/+* GC had significantly less Mitotracker@ Green signal per cell than WT cells (Fig. 3C; $P < 0.05$, signal plotted after normalization to WT fluorescence where mean WT fluorescence was set to 1), and that *PM/PM* cells showed diminished (but not statistically significant) signal. That both PM genotypes exhibited reduced mitochondrial mass in this experiment was consistent with the detected reduction in mtDNA copy number (above).

While evaluating the flow cytometric histogram plots, we noted an interesting and important difference in the fluorescence distribution of PM cells compared with WT cells. Figure 3D and E shows example flow cytometric histogram plots of Mitotracker@ Green fluorescence

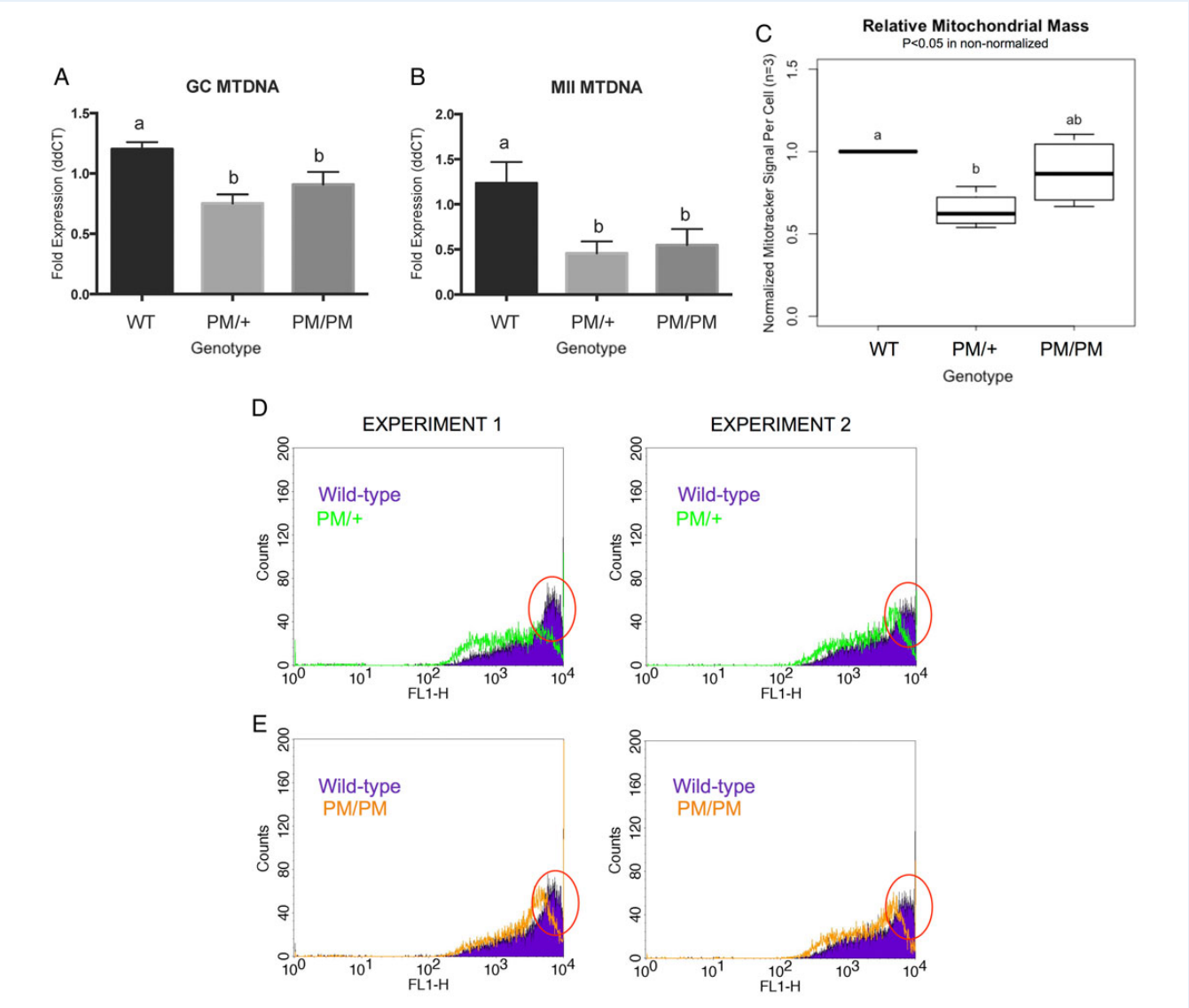

Figure 3 Analysis of mitochondrial number and mass in FXPM animals versus controls. First, qPCR of mitochondrial DNA was determined by amplification of the mitochondrial *Cox I* gene and calculating ddCT values using *β-globin* as the housekeeping control ($n = 4$ samples per genotype). Mitochondrial DNA copy number was determined in GC (**A**) and MII eggs (**B**; MII). Statistically different means, are denoted by letters 'a' and 'b' ($P < 0.05$, ANOVA). Mitochondrial mass was also determined by staining cells with the mitochondria-specific fluorescent molecule Mitotracker@ green and measuring signal using a flow cytometer (**C**; $n = 4$ samples per genotype). Relative mean fluorescence is depicted as compared with WT signal normalized to 1. Significantly reduced signal ($P < 0.05$) was found in *PM/+* GC versus WT, while *PM/PM* GC showed a slight but non-significant decrease. Flow cytometric results of two unique experiments are shown in (**D**; WT, purple versus *PM/+*, green) and (**E**; WT, purple versus *PM/PM*, orange). A peak of highly fluorescent cells was seen in WT samples that was missing from each of the FXPM mutant samples (red ovals).

in two unique experiments (of 3). WT signal is shown in each case in purple, while *PM/+* is overlaid in green (top plots) and *PM/PM* is overlaid in orange (bottom plots). Strikingly, fluorescence events for WT cells (processed identically to PM cells) exhibited a histogram peak near 10^4 relative fluorescence units that was lacking in cells of both PM genotypes. This means that the fraction of WT cells with the greatest Mitotracker@ Green signal, and therefore the greatest mitochondrial mass per cell, is missing in the mutant cumulus GC. Instead, more mutant cells exhibit the lower end of the range of fluorescence. This is of course consistent with the reduced mean fluorescence (Fig. 3C) of all cells, and also with the reduced mtDNA copy number (Fig. 3A and B). These data together caused us to ask whether mitochondrial structure might be altered in FXPM mice.

To evaluate the fine structure of GC mitochondria, transmission electron microscopy (TEM) was performed on ovary preparations of each genotype. Here, we evaluated the mitochondria of intact GC within pre-antral follicles (Table III). Mitochondria with normal, stereotypical appearance were noted in each WT region assessed (Fig. 4A, green ovals, note the organized appearance of normal mitochondrial cristae with many parallel membrane layers). Further, the dual rings indicative

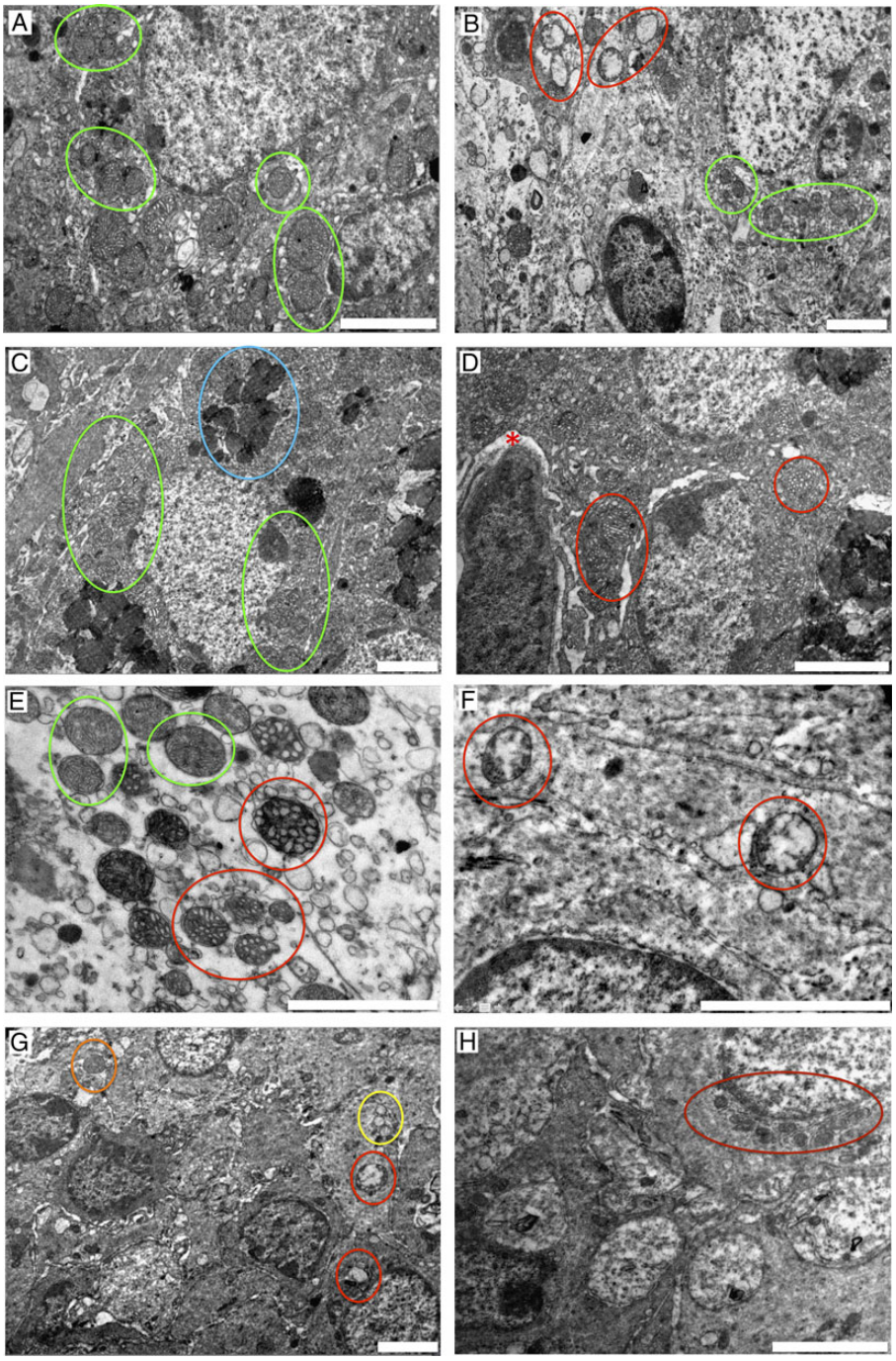

Figure 4 Transmission electron microscopic analysis of WT, *PM/+* and *PM/PM* GC. Representative images from pre-antral follicles from three ovary samples per genotype are shown; all scale bars are 2 μm and magnification is as indicated here in the legend for each panel. (**A**) shows a micro-graph from a representative WT GC with normal mitochondria in terms of size and the appearance of cristae (green ovals; × 10 000 magnification). Normal WT mitochondria are also shown in (**B**; green ovals; ×6300), with some mitochondria undergoing recycling (red ovals). Normal mitochondria are also found in *PM/+* follicles (**C**; green ovals; ×6300), along with dark, abnormal mitochondria with few cristae (C; blue oval). The inner compartment of these mitochondria is filled with a closely packed array of dense ribbons, which impart an overall dense appearance to the mitochondrial matrix. *PM/+* GC also contain mitochondria with 'tubular' cristae in cross section (**D**; red ovals; × 10 000) and intracellular space (asterisk) not seen in WT GC. A *PM/+* GC region with highly abnormal 'honeycomb' mitochondria is shown in (**E**; red ovals; × 16 000), with some mitochondria with relatively normal cristae but some signs of disorganization (green ovals) nearby. *PM/+* GC mitochondria are also seen (**F**, ×20 000; **G**, ×6300) with short cristae that are entirely restricted to the mitochondrial periphery. The inner compartment is occupied by a vastly augmented matrix of normal electron density but some contain numerous dense bodies (red ovals) and (G; *PM/PM*, red ovals). *PM/PM* GC also contain mitochondria with a vacuolated internal cristae appearance (G; yellow oval), dark appearance (G; orange oval), and a 'blurred' compact appearance (**H**; red oval; × 12 500).

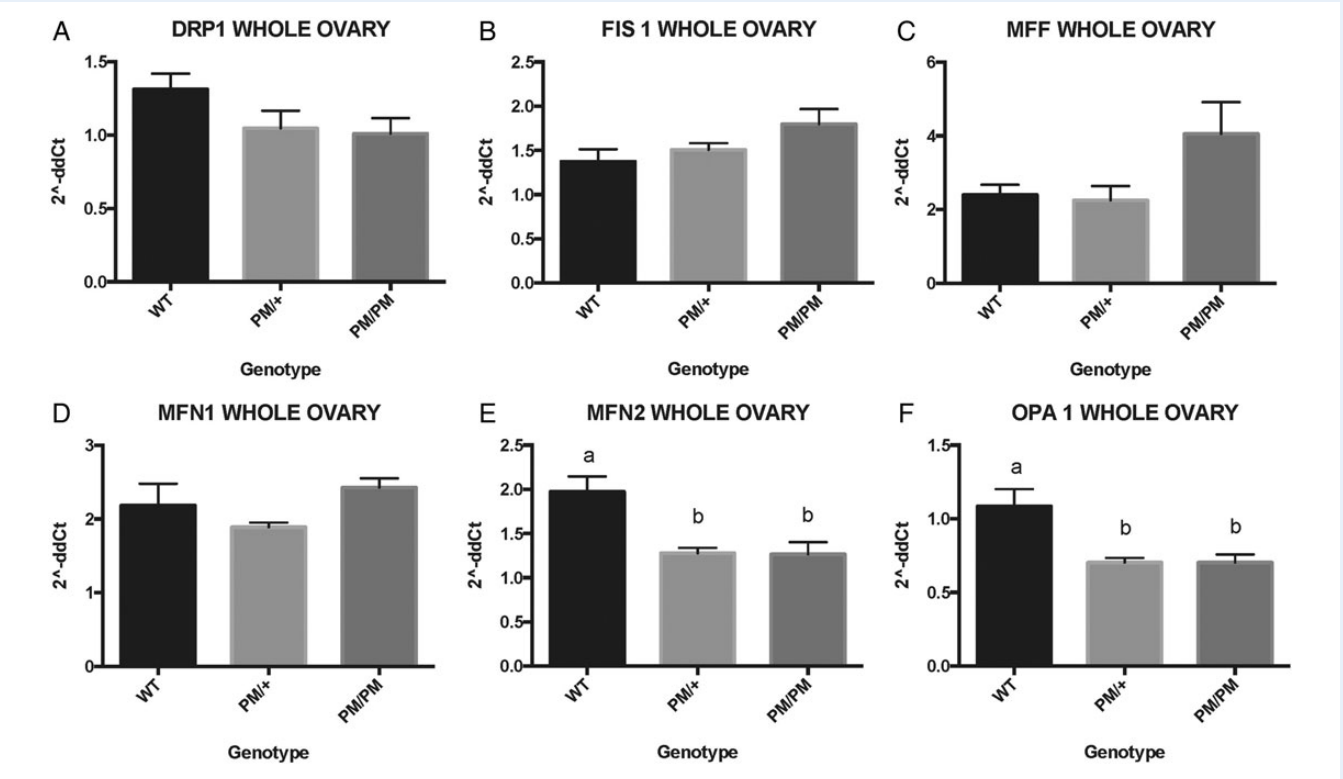

Figure 5 qRT–PCR gene expression analysis in whole ovaries. Expression of six genes involved in the control of mitochondrial structure or recycling (*Drp1* - panel **A**, *Fis1* - **B**, *Mff* - **C**; *Mfn1* - **D**, *Mfn2* - **E**; *Opa1* - **F**) was measured. Two genes (*Mfn2*, *Opa1*) showed significantly different expression between WT and mutant ovaries (panels E, F; a minimum of three experimental cDNA replicates were used per genotype; statistically different means, are denoted by letters 'a', 'b', and optionally 'c', $P < 0.05$, as determined by ANOVA analysis); those were reduced in the mutants.

of mitochondrial recycling/mitophagy (Czaja *et al.*, 2014) (Fig. 4B; red ovals, see also normal mitochondria in green ovals in same panel) were also easily identifiable in the WT sections.

Mitochondria with normal appearance(s) were also visible in *PM/+* and *PM/PM* TEM preparations (Example, Fig. 4C, green ovals). However, strikingly abnormal mitochondria were also present in mutant preparations. Mitochondrial cristae were often thicker and distended, with an appearance we referred to as 'honeycombs.' In these organelles, mitochondrial structure was a 'tubular' type, characterized by many tubules approximately 500 Å wide, which to a large extent replaced the normal cristae. Because the tubules were densely packed and occupied the majority of the mitochondrial volume, the cross-sectioned area had a honeycomb-like appearance (Fig. 4D and E normal—green oval, abnormal—red ovals) compared with the organized/parallel nature of the cristae of normal mitochondria. *PM/+* samples and also *PM/PM* samples also exhibited irregular intracellular spaces (Fig. 4D, asterisk) that were not seen in WT controls. Additional abnormalities were found in the mitochondria of mutant GC that were absent from WT mitochondria. In Fig. 4F and G, mitochondria with very sparse/absent cristae are shown in *PM/+* and *PM/PM* samples, respectively (red ovals) and 4G also includes an example mitochondrion with a 'vacuolated' appearance (yellow oval) and an example with a 'dark/ghostlike' appearance (orange oval). In this last case, mitochondria have an augmented matrix and a sparsity of cristae. When present, cristae are abnormally short and peripherally located, leaving the center of the organelles devoid of membranes and occupied by a structureless matrix that lacks inclusions of any sort. Figure 4H shows more examples of dark/ghostlike mitochondria in a *PM/PM* GC. All of the above examples of abnormal mitochondrial morphology were not present in WT GC. Evaluation of these electron micrographs led us to hypothesize that the expression of genes that control mitochondrial structure and in some cases, recycling, would be altered in the presence of the FXPM.

To begin to determine mechanisms by which mitochondrial mass and structure (and possibly function) were altered by the PM, we carried out gene expression analyses on whole ovary, GC, and oocyte samples collected from each genotype. Figure 5 shows the result of quantitative reverse transcription/PCR (qRT-PCR) gene expression analysis in whole ovaries of 6 week-old animals. We selected six genes, each of which encode proteins in either mitochondrial structure or recycling (A-F; *dynamin-related protein 1—Drp1* (Frank *et al.*, 2001; Zhang *et al.*, 2015); *Fission 1—Fis1* (Zhang *et al.*, 2015); *mitochondrial fission factor—Mff* (Otera and Mihara, 2011; Zhang *et al.*, 2015); *mitofusin 1* and *2—Mfn1*, *Mfn2* (Chen *et al.*, 2003, 2010; Ishihara *et al.*, 2004); *optic atrophy 1—Opa 1* (Zorzano and Claret, 2015)). Expression was normalized using the concurrent measurement of β-actin. Two of these genes, *Mfn2* and *Opa1*, showed significantly reduced expression in the ovaries of both *PM/+* and *PM/PM* animals compared with WT.

Next, we asked whether the expression of any of these genes differed between the genotypes in isolated cumulus GC, or, in isolated

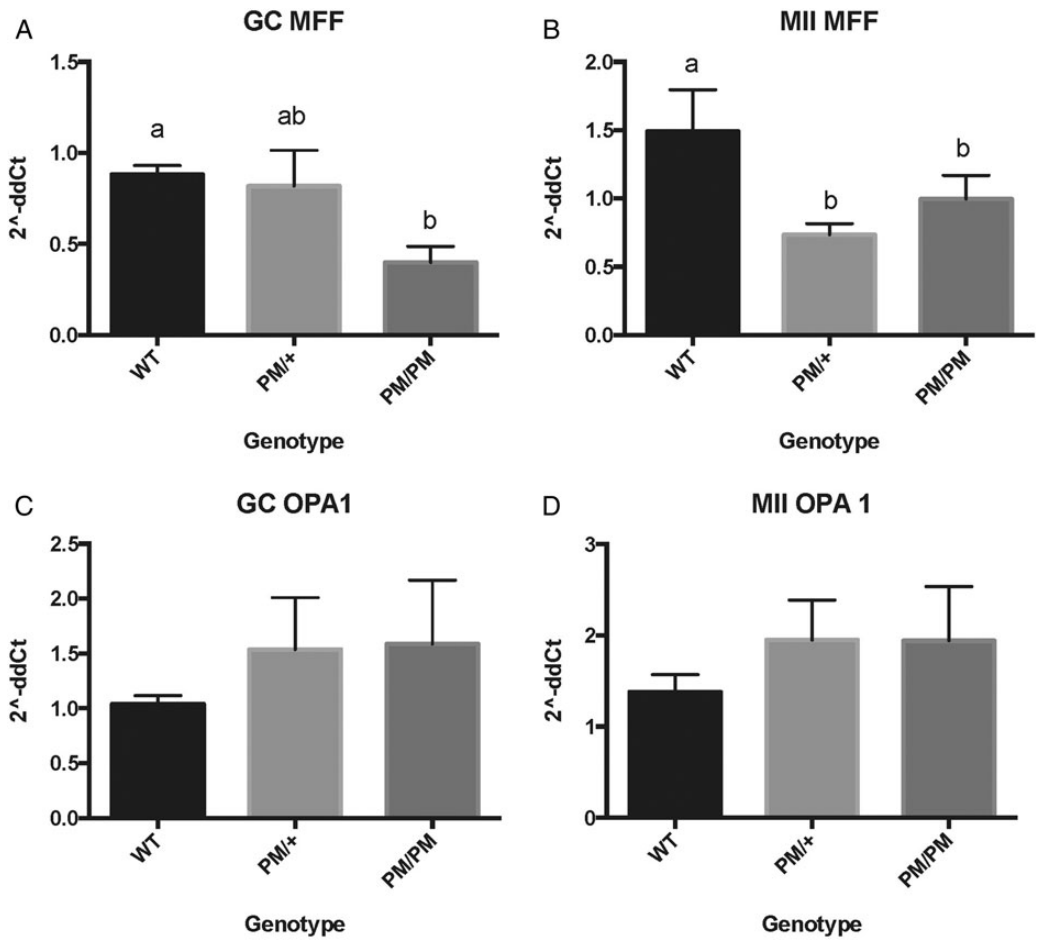

Figure 6 qRT–PCR gene expression analysis in cumulus GC and metaphase II eggs. Of the mitochondrial structural genes evaluated in GC and eggs, only *Mff* showed significantly altered expression, and here, was reduced in *PM/PM* GC (**A**), and in both *PM/+* GC and *PM/PM* eggs (**B**) ($P < 0.05$, ANOVA). *Opa1* (**C**, **D**) did not exhibit statistically significant differences in expression (A minimum of three experimental cDNA replicates were used per genotype).

metaphase II eggs (Fig. 6). qRT–PCR analysis of cumulus GC revealed that of *Drp1*, *Fis1*, *Mff*, *Mfn2*, *Opa1*, only *Mff* (A) showed significantly decreased expression (as seen in whole ovary), and here, only the *PM/PM* cells exhibited the reduced expression compared with WT cells. *Mff* expression was also significantly decreased in metaphase II eggs of heterozygote and homozygote mice (B). While it is highly likely that other genes not assessed in these studies are also dysregulated, we now hypothesize that the aberrant mitochondrial architecture shown in our electron micrographs (Fig. 4), and possibly the reduction in mitochondrial mass (Fig. 3) seen in FXPM mutant GC results at least in part from this reduction in *Mff* expression. How much of the FXPOI phenotype is attributable to GC or oocyte mitochondrial abnormalities remains to be determined.

Discussion

Here we show that that the FXPM 130R mice have lower fecundity, fewer CL and increased atresia of large antral follicles, findings that were more pronounced in mice homozygous for the PM than mice that are heterozygous. Interestingly, the inter-replicate variability of follicles, CL, and ZPR was increased in PM animals. Furthermore, GC and MII eggs of PM mice exhibit mitochondrial abnormalities that include a lower than normal mtDNA copy number and lower mitochondrial mass (in ovulated cumulus GC). In addition, many mitochondria in the follicular GC of PM mice showed highly aberrant morphology, including those that contained extra-dense 'honeycomb' internal cristae, those that were vacuolated, and others that lacked cristae and had an 'empty' appearance.

It is evident from our and other studies that structural abnormalities of mitochondria represent more than a curiosity *per se*, and are instead pathognomonic of metabolic perturbations (Luft *et al.*, 1962; Tandler and Hoppel, 1980; Riva *et al.*, 2006; Fujioka *et al.*, 2014) that relate to mitochondria inner membrane organization and function. Indeed, altered mitochondria morphology and bioenergetics has been observed in other studies using fibroblasts and postmortem brain samples from premutation carriers as well as from a knock-in (KI) mouse model (Napoli *et al.*, 2011; Kaplan *et al.*, 2012b). A preliminary assessment of the expression of key mitochondrial structural genes followed to begin to determine why these structural abnormalities were occurring.

In whole ovaries, the expression of two genes involved in the regulation of mitochondrial structure (*Mfn2, Opa1*) was significantly lower in PM mice. Thus a novel consequence of the PM in either a heterozygous or homozygous state is the dysregulation of the expression of some

important mitochondrial genes in the whole ovary. In isolated cumulus GC, only *Mff* showed significantly decreased expression and here, only the homozygous PM mice exhibited the reduced expression compared with WT cells). *Mff* expression was also significantly decreased in metaphase II eggs of both heterozygous and homozygous PM mice.

Otera *et al.* (Otera and Mihara, 2011) showed that knockdown of the genes *Opa1* and *Drp1* in combination, or knockdown of *Opa1* and *Mff*, both resulted in mitochondrial cristae that resemble the 'honeycomb' mitochondrial cristae we observed in FXPM GC. Knockdown of *Opa1* either alone, or in combination with *Fis1* resulted in smaller mitochondria with an 'empty' appearance as seen in the mice with the PM. Thus our gene expression studies are consistent with a model in which the FXPM allele results in aberrant expression of these mitochondrial fission genes (including, but not limited to *Mff*), resulting in dysfunctional mitochondria that in turn may negatively impact follicle viability.

The difference in gene expression seen in the total ovary, where four genes are dysregulated, and in the cumulus GC and eggs, where only *Mff* is dysregulated, may reflect the fact that the ovary contains a diversity of many cell types, in ratios that depend on follicle growth. That is, when many large follicles are present, the ratio of GC and growing oocytes to the rest of the ovary is quite high. When few large follicles are present, GC and growing oocytes are present only in a small fraction relative to the other somatic cell types of the organ, the bulk of which is connective stroma. Each of these cell types may be affected by the FXPM in different ways, and continuing studies are needed to determine broader effects of the PM mitochondrial regulatory gene expression in the follicle.

Comparison and contrast between the ovarian phenotypes of the FXPM 130R mouse (Hoffman *et al.*, 2012; Lu *et al.*, 2012) studied here, the exCGG-KI 'Dutch knock-in' PM mouse (Bontekoe *et al.*, 2001; Willemsen *et al.*, 2003; Brouwer *et al.*, 2007), and a Fragile X mental retardation 1 (Fmr1) knockout mouse (Ascano *et al.*, 2012) allow us to interpret the ovarian compromise detected as resulting from the 'toxic' PM transcript itself. With regards to the potentially-toxic FMRPolyG protein (Todd *et al.*, 2013; Oh *et al.*, 2015), a recent report by Buijsen *et al.* (2015) is enlightening. Their analysis of the Dutch knock-in mouse strain (Bontekoe *et al.*, 2001; Willemsen *et al.*, 2003; Brouwer *et al.*, 2007) that produces both PM RNA and FMRPolyG, revealed similar effects of that PM allele upon follicle and CL development as shown here. FMRPolyG protein inclusions were detected not only in the stromal cells of PM mouse ovaries, but also in the stromal cells of ovarian tissue from a human PM carrier. FMRPolyG inclusions were not detected in the oocytes, GC, or theca cells of the Dutch knock-in PM ovaries. Because of this, and the lack of detection of the FMRPolyG inclusions in our FXPM 130R mice, we attribute our detected phenotype as mainly depending upon the PM transcript. Low levels of FMRPolyG RAN protein (e.g. below the level required to give rise to subcellular inclusions (Todd *et al.*, 2013)) may contribute to the broader FXPOI condition, but it appears that the PM transcript itself is associated with pathology. Last, while it is true that *PM/+* ovaries have been shown to produce lower levels of Fmr1 protein FMRP, *Fmr1* deletion has instead been shown to be associated with precocious follicle growth and possible ovary hyperplasia (Ascano *et al.*, 2012) rather than any increase in follicle death. One might therefore not expect mitochondrial abnormalities and ovarian compromise to result from lower levels of ovarian FMRP. Instead, our data support a model where the *FMR1* PM transcript itself contributes to the mitochondrial and ovarian abnormalities we have characterized.

The inter-replicate variability of histomorphometric measurements in PM ovaries was striking. As mentioned, only a subset of women that carry the PM exhibit signs of accelerated ovarian demise (Welt *et al.*, 2004) and accordingly, only a subset of female PM carriers exhibit signs of Fragile X Tremor and Ataxia Syndrome (FXTAS) (Coffey *et al.*, 2008). The variability in the number of immature follicles seen in both heterozygous and homozygous animal is reminiscent of incomplete penetrance of FXPOI and FXTAS in human carriers. Detection of this variance in an inbred strain of mice suggests that the PM can have variable impact in the absence of coincident genetic modifiers. This will be investigated further in ongoing studies. As far as the acute impact of the PM on growing follicles, it is as yet unclear exactly why the cell and follicle death phenotype only becomes consistent when follicles reach the antral stages in our mouse model. This may result from the time of exposure to the 'toxic' CGG-containing RNA (Handa *et al.*, 2005; McLeod *et al.*, 2005; Wojciechowska and Krzyzosiak, 2011; Hagerman and Hagerman, 2013) over the course of follicle growth. The effects of the PM on mitochondrial content and structure found in cells of the ovary may be representative of a more general, widespread mitochondrial phenotype in PM carriers. Comparison of cumulus cell mitochondria between PM carrier and non-carrier women undergoing IVF cycles will reveal whether mitochondrial dysfunction also occurs in the human condition of FXPOI, with potential consequences for fertility and fecundity.

Acknowledgements

Dr. Hugh Taylor is gratefully acknowledged for experimental consultation and comments on the manuscript while in preparation.

Authors' roles

Study execution: J.J. and C.C.D. designed the studies; C.C.D., B.U., M.H., D.-Q.M., and M.K. performed experiments; M.K. and M.G. processed samples and prepared electron micrographs, C.G. interpreted electron micrographs; S.B. and A.S. assisted with flow cytometry. Manuscript preparation: J.J. and K.U. wrote the manuscript, G.H., C.G., L.D.S, and M.F. provided scientific and editorial feedback on manuscript.

Funding

These studies were supported by National Institutes of Health (NIH) R21 071873 (J.J., G.H.), The Albert McKern Fund for Perinatal Research (J.J.), NIH Intramural Funds (K.U.), and a TUBITAK Research Fellowship Award (B.U.).

Conflict of interest

None declared.

References

Addabbo F, Ratliff B, Park HC, Kuo MC, Ungvari Z, Csiszar A, Ciszar A, Krasnikov B, Krasnikof B, Sodhi K *et al.* The Krebs cycle and mitochondrial mass are early victims of endothelial dysfunction: proteomic approach. *Am J Pathol* 2009;**174**:34–43.

Albertini DF, Barrett SL. Oocyte-somatic cell communication. *Reprod Suppl*2003;**61**:49–54.

Allen EG, Sullivan AK, Marcus M, Small C, Dominguez C, Epstein MP, Charen K, He W, Taylor KC, Sherman SL. Examination of reproductive aging milestones among women who carry the FMR1 premutation. *Hum Reprod*2007;**22**:2142–2152.

Ascano M, Mukherjee N, Bandaru P, Miller JB, Nusbaum JD, Corcoran DL, Langlois C, Munschauer M, Dewell S, Hafner M *et al.* FMRP targets distinct mRNA sequence elements to regulate protein expression. *Nature* 2012;**492**:382–386.

Behrman HR, Kodaman PH, Preston SL, Gao S. Oxidative stress and the ovary. *J Soc Gynecol Investig* 2001;**8**:S40–S42.

Bontekoe CJ, Bakker CE, Nieuwenhuizen IM, van der Linde H, Lans H, de Lange D, Hirst MC, Oostra BA. Instability of a (CGG)98 repeat in the Fmr1 promoter. *Hum Mol Genet* 2001;**10**:1693–1699.

Boucret L, Chao de la Barca JM, Morinière C, Desquiret V, Ferré-L'Hôtellier V, Descamps P, Marcaillou C, Reynier P, Procaccio V, May-Panloup P. Relationship between diminished ovarian reserve and mitochondrial biogenesis in cumulus cells. *Hum Reprod* 2015;**30**:1653–1664.

Brouwer JR, Mientjes EJ, Bakker CE, Nieuwenhuizen IM, Severijnen LA, Van der Linde HC, Nelson DL, Oostra BA, Willemsen R. Elevated Fmr1 mRNA levels and reduced protein expression in a mouse model with an unmethylated Fragile X full mutation. *Exp Cell Res* 2007;**313**:244–253.

Buijsen RA, Visser JA, Kramer P, Severijnen EA, Gearing M, Charlet-Berguerand N, Sherman SL, Berman RF, Willemsen R, Hukema RK. Presence of inclusions positive for polyglycine containing protein, FMRpolyG, indicates that repeat-associated non-AUG translation plays a role in fragile X-associated primary ovarian insufficiency. *Hum Reprod* 2015;**31**:158–168.

Carlson JC, Wu XM, Sawada M. Oxygen radicals and the control of ovarian corpus luteum function. *Free Radic Biol Med* 1993;**14**:79–84.

Chen H, Detmer SA, Ewald AJ, Griffin EE, Fraser SE, Chan DC. Mitofusins Mfn1 and Mfn2 coordinately regulate mitochondrial fusion and are essential for embryonic development. *J Cell Biol* 2003;**160**:189–200.

Chen H, Vermulst M, Wang YE, Chomyn A, Prolla TA, McCaffery JM, Chan DC. Mitochondrial fusion is required for mtDNA stability in skeletal muscle and tolerance of mtDNA mutations. *Cell* 2010; **141**:280–289.

Coffey SM, Cook K, Tartaglia N, Tassone F, Nguyen DV, Pan R, Bronsky HE, Yuhas J, Borodyanskaya M, Grigsby J *et al.* Expanded clinical phenotype of women with the FMR1 premutation. *Am J Med Genet A* 2008; **146A**:1009–1016.

Czaja MJ, Ding WX, Donohue TM, Friedman SL, Kim JS, Komatsu M, Lemasters JJ, Lemoine A, Lin JD, Ou JhJ *et al.* Functions of autophagy in normal and diseased liver. *Autophagy* 2014;**9**:1131–1158.

de Lamirande E, Gagnon C. Reactive oxygen species (ROS) and reproduction. *Adv Exp Med Biol* 1994;**366**:185–197.

Frank S, Gaume B, Bergmann-Leitner ES, Leitner WW, Robert EG, Catez F, Smith CL, Youle RJ. The role of dynamin-related protein 1, a mediator of mitochondrial fission, in apoptosis. *Dev Cell* 2001;**1**:515–525.

Fujioka H, Tandler B, Cohen M, Koontz D, Hoppel CL. Multiple mitochondrial alterations in a case of myopathy. *Ultrastruct Pathol*2014; **38**:204–210.

Hagerman R, Hagerman P. Advances in clinical and molecular understanding of the FMR1 premutation and fragile X-associated tremor/ataxia syndrome. *Lancet Neurol* 2013;**12**:786–798.

Handa V, Goldwater D, Stiles D, Cam M, Poy G, Kumari D, Usdin K. Long CGG-repeat tracts are toxic to human cells: implications for carriers of Fragile X premutation alleles. *FEBS Lett* 2005;**579**:2702–2708.

Hoffman GE, Le WW, Entezam A, Otsuka N, Tong ZB, Nelson L, Flaws JA, McDonald JH, Jafar S, Usdin K. Ovarian abnormalities in a mouse model of fragile X primary ovarian insufficiency. *J Histochem Cytochem* 2012; **60**:439–456.

Hukema RK, Buijsen RA, Raske C, Severijnen LA, Nieuwenhuizen-Bakker I, Minneboo M, Maas A, de Crom R, Kros JM, Hagerman PJ *et al.* Induced expression of expanded CGG RNA causes mitochondrial dysfunction in vivo. *Cell Cycle* 2014;**13**:2600–2608.

Ishihara N, Eura Y, Mihara K. Mitofusin 1 and 2 play distinct roles in mitochondrial fusion reactions via GTPase activity. *J Cell Sci* 2004; **117**:6535–6546.

Johnson J, Canning J, Kaneko T, Pru JK, Tilly JL. Germline stem cells and follicular renewal in the postnatal mammalian ovary. *Nature* 2004; **428**:145–150.

Kaplan ES, Cao Z, Hulsizer S, Tassone F, Berman RF, Hagerman PJ, Pessah IN. Early mitochondrial abnormalities in hippocampal neurons cultured from Fmr1 pre-mutation mouse model. *J Neurochem* 2012a;**123**:613–621.

Kaplan ES, Cao Z, Hulsizer S, Tassone F, Berman RF, Hagerman PJ, Pessah IN. Early mitochondrial abnormalities in hippocampal neurons cultured from Fmr1 pre-mutation mouse model. *J Neurochem* 2012b;**123**:613–621.

Karuputhula NB, Chattopadhyay R, Chakravarty B, Chaudhury K. Oxidative status in granulosa cells of infertile women undergoing IVF. *Syst Biol Reprod Med* 2013;**59**:91–98.

Lu C, Lin L, Tan H, Wu H, Sherman SL, Gao F, Jin P, Chen D. Fragile X premutation RNA is sufficient to cause primary ovarian insufficiency in mice. *Hum Mol Genet* 2012;**21**:5039–5047.

Luderer U. Ovarian toxicity from reactive oxygen species. *Vitam Horm* 2014; **94**:99–127.

Luft R, Ikkos D, Palmieri G, Ernster L, Afzelius B. A case of severe hypermetabolism of nonthyroid origin with a defect in the maintenance of mitochondrial respiratory control: a correlated clinical, biochemical, and morphological study. *J Clin Invest* 1962;**41**:1776–1804.

McLeod CJ, O'Keefe LV, Richards RI. The pathogenic agent in Drosophila models of 'polyglutamine' diseases. *Hum Mol Genet* 2005;**14**:1041–1048.

Murray A, Webb J, Grimley S, Conway G, Jacobs P. Studies of FRAXA and FRAXE in women with premature ovarian failure. *J Med Genet* 1998; **35**:637–640.

Myers M, Britt KL, Wreford NGM, Ebling FJP, Kerr JB. Methods for quantifying follicular numbers within the mouse ovary. *Reproduction* 2004;**127**:569–580.

Napoli E, Ross-Inta C, Wong S, Omanska-Klusek A, Barrow C, Iwahashi C, Garcia-Arocena D, Sakaguchi D, Berry-Kravis E, Hager- man R *et al.* Altered zinc transport disrupts mitochondrial protein processing/import in fragile X-associated tremor/ataxia syndrome. *Hum Mol Genet* 2011; **20**:3079–3092.

Oh SY, He F, Krans A, Frazer M, Taylor JP, Paulson HL, Todd PK. RAN translation at CGG repeats induces ubiquitin proteasome system impairment in models of fragile X-associated tremor ataxia syndrome. *Hum Mol Genet* 2015;**24**:4317–4326.

Otera H, Mihara K. Discovery of the membrane receptor for mitochondrial fission GTPase Drp1. *Small GTPases* 2011;**2**:167–172.

Pastore LM, Johnson J. The FMR1 gene, infertility, and reproductive decision-making: a review. *Front Genet* 2014;**5**:195.

Pieretti M, Zhang FP, Fu YH, Warren ST, Oostra BA, Caskey CT, Nelson DL. Absence of expression of the FMR-1 gene in fragile X syndrome. *Cell* 1991; **66**:817–822.

R Core Team. 2014. *R: A Language and Environment for Statistical Computing*. Vienna, Austria: R Foundation for Statistical Computing.

Riva A, Tandler B, Lesnefsky EJ, Conti G, Loffredo F, Vazquez E, Hoppel CL. Structure of cristae in cardiac mitochondria of aged rat. *Mech Ageing Dev* 2006;**127**:917–921.

Ross-Inta C, Omanska-Klusek A, Wong S, Barrow C, Garcia-Arocena D, Iwahashi C, Berry-Kravis E, Hagerman RJ, Hagerman PJ, Giulivi C. Evidence of mitochondrial dysfunction in fragile X-associated tremor/ ataxia syndrome. *Biochem J* 2010;**429**:545–552.

Sahin E, Colla S, Liesa M, Moslehi J, Muller FL, Guo M, Cooper M, Kotton D, Fabian AJ, Walkey C *et al.* Telomere dysfunction induces metabolic and mitochondrial compromise. *Nature*2011;**470**:359–365.

Seino T, Saito H, Kaneko T, Takahashi T, Kawachiya S, Kurachi H. Eight-hydroxy-2'-deoxyguanosine in granulosa cells is correlated with the quality of oocytes and embryos in an in vitro fertilization-embryo transfer program. *Fertil Steril* 2002;**77**:1184–1190.

Sellier C, Rau F, Liu Y, Tassone F, Hukema RK, Gattoni R, Schneider A, Richard S, Willemsen R, Elliott DJ *et al.* Sam68 sequestration and partial loss of function are associated with splicing alterations in FXTAS patients. *EMBO J* 2010;**29**:1248–1261.

Sellier C, Freyermuth F, Tabet R, Tran T, He F, Ruffenach F, Alunni V, Moine H, Thibault C, Page A *et al.* Sequestration of DROSHA and DGCR8 by expanded CGG RNA repeats alters microRNA processing in fragile X-associated tremor/ataxia syndrome. *Cell Rep* 2013; **3**:869–880.

Sutcliffe JS, Nelson DL, Zhang F, Pieretti M, Caskey CT, Saxe D, Warren ST. DNA methylation represses FMR-1 transcription in fragile X syndrome. *Hum Mol Genet* 1992;**1**:397–400.

Tandler B, Hoppel CL. Ultrastructural effects of riboflavin deficiency on rat hepatic mitochondria. *Anat Rec* 1980;**196**:183–190.

Tassone F, Hagerman RJ, Loesch DZ, Lachiewicz A, Taylor AK, Hagerman PJ. Fragile X males with unmethylated, full mutation trinucleotide repeat expansions have elevated levels of FMR1 messenger RNA. *Am J Med Genet* 2000;**94**:232–236.

Tassone F, Beilina A, Carosi C, Albertosi S, Bagni C, Li L, Glover K, Bentley D, Hagerman PJ. Elevated FMR1 mRNA in premutation carriers is due to increased transcription. *RNA* 2007;**13**:555–562.

Tilly JL. Ovarian follicle counts—not as simple as 1, 2, 3. *Reprod Biol Endocrinol* 2003;**1**:11.

Todd PK, Oh SY, Krans A, He F, Sellier C, Frazer M, Renoux AJ, Chen KC, Scaglione KM, Basrur V *et al.* CGG repeat-associated translation mediates neurodegeneration in fragile X tremor ataxia syndrome. *Neuron* 2013;**78**:440–455.

Tokmak A, Yldrm G, Sarkaya E, Ç nar M, Bŏgdaycŏglu N, Ylmaz FM, Ylmaz N. Increased oxidative stress markers may be a promising indicator of risk for primary ovarian insufficiency: a cross-sectional case control study. *Rev Bras Ginecol Obstet* 2015;**37**:411–416.

Van Blerkom J. Mitochondria in human oogenesis and preimplantation embryogenesis: engines of metabolism, ionic regulation and developmental competence. *Reproduction* 2004;**128**:269–280.

Van Blerkom J. Mitochondrial function in the human oocyte and embryo and their role in developmental competence. *Mitochondrion* 2011;**11**:797–813.

Welt CK, Smith PC, Taylor AE. Evidence of early ovarian aging in fragile X premutation carriers. *J Clin Endocrinol Metab* 2004;**89**:4569–4574.

Wigglesworth K, Lee KB, Emori C, Sugiura K, Eppig JJ. Transcriptomic diversification of developing cumulus and mural granulosa cells in mouse ovarian follicles. *Biol Reprod* 2015;**92**:23.

Willemsen R, Hoogeveen-Westerveld M, Reis S, Holstege J, Severijnen LA, Nieuwenhuizen IM, Schrier M, van Unen L, Tassone F, Hoogeveen AT *et al.* The FMR1 CGG repeat mouse displays ubiquitin-positive intranuclear neuronal inclusions; implications for the cerebellar tremor/ataxia syndrome. *Hum Mol Genet* 2003;**12**:949–959.

Wojciechowska M, Krzyzosiak WJ. Cellular toxicity of expanded RNA repeats: focus on RNA foci. *Hum Mol Genet* 2011;**20**:3811–3821.

Zhang Z, Liu L, Wu S, Xing D. Drp1, Mff, Fis1, and MiD51 are coordinated to mediate mitochondrial fission during UV irradiation- induced apoptosis. *FASEB J* 2015;**30**:466–476.

Zorzano A, Claret M. Implications of mitochondrial dynamics on neurodegeneration and on hypothalamic dysfunction. *Front Aging Neurosci* 2015;**7**:101.